Mutations in Radial Spoke Head Protein Genes *RSPH9* and *RSPH4A* Cause Primary Ciliary Dyskinesia with Central-Microtubular-Pair Abnormalities

Victoria H. Castleman,[1,13] Leila Romio,[2] Rahul Chodhari,[1] Robert A. Hirst,[3] Sandra C.P. de Castro,[4] Keith A. Parker,[1] Patricia Ybot-Gonzalez,[4] Richard D. Emes,[5] Stephen W. Wilson,[6] Colin Wallis,[7] Colin A. Johnson,[8] Rene J. Herrera,[9] Andrew Rutman,[3] Mellisa Dixon,[10] Amelia Shoemark,[10] Andrew Bush,[10] Claire Hogg,[10] R. Mark Gardiner,[1] Orit Reish,[11] Nicholas D.E. Greene,[4] Christopher O'Callaghan,[3] Saul Purton,[12] Eddie M.K. Chung,[1] and Hannah M. Mitchison[1,*]

Primary ciliary dyskinesia (PCD) is a genetically heterogeneous inherited disorder arising from dysmotility of motile cilia and sperm. This is associated with a variety of ultrastructural defects of the cilia and sperm axoneme that affect movement, leading to clinical consequences on respiratory-tract mucociliary clearance and lung function, fertility, and left-right body-axis determination. We performed whole-genome SNP-based linkage analysis in seven consanguineous families with PCD and central-microtubular-pair abnormalities. This identified two loci, in two families with intermittent absence of the central-pair structure (chromosome 6p21.1, Zmax 6.7) and in five families with complete absence of the central pair (chromosome 6q22.1, Zmax 7.0). Mutations were subsequently identified in two positional candidate genes, *RSPH9* on chromosome 6p21.1 and *RSPH4A* on chromosome 6q22.1. Haplotype analysis identified a common ancestral founder effect *RSPH4A* mutation present in UK-Pakistani pedigrees. Both *RSPH9* and *RSPH4A* encode protein components of the axonemal radial spoke head. In situ hybridization of murine *Rsph9* shows gene expression restricted to regions containing motile cilia. Investigation of the effect of knockdown or mutations of *RSPH9* orthologs in zebrafish and *Chlamydomonas* indicate that radial spoke head proteins are important in maintaining normal movement in motile, "9+2"-structure cilia and flagella. This effect is rescued by reintroduction of gene expression for restoration of a normal beat pattern in zebrafish. Disturbance in function of these genes was not associated with defects in left-right axis determination in humans or zebrafish.

Introduction

Primary ciliary dyskinesia (PCD, MIM 242650) refers to a heterogeneous group of genetic ciliopathies characterized by ultrastructural defects in the axonemal structure of "9+2" motile cilia and sperm flagella.[1] The incidence is estimated at 1:15,000–30,000,[2] with higher incidence in certain consanguineous and isolated populations.[3,4] Clinical features reflect the distribution of dysmotile cilia in the body and include neonatal respiratory distress, chronic respiratory infections, sinusitis, and bronchiectasis, due to deficient cilia function in the upper and lower airways. Male and female subfertility occurs as a result of defective sperm flagella and oviduct cilia, respectively. There is occasional hydrocephalus as a result of deficient ependymal cilia.[5,6] In most families, there is apparent randomization of left-right axis development, proposed to result from defective function of embryonic nodal cilia.[7,8] This manifests in about half of patients as *situs inversus* or more severe laterality defects, such as cardiovascular abnormalities.

PCD is usually recessively inherited, and five PCD genes have been identified: *DNAI1* (MIM 604366), *DNAH5* (MIM 603335), *DNAH11* (MIM 603339), *DNAI2* (MIM 605483)[9] and *TXNDC3* (MIM 607421) (reviewed by Bush et al.[10]). These encode axonemal dyneins and are associated with reduction or loss of axonemal outer dynein arms, which are the multisubunit axonemal ATPase complexes that generate the force for cilia motility and govern beat frequency. *DNAH5* and *DNAI1* are a relatively more common cause of disease, underlying an estimated 28% (*DNAH5*[11]) and 2%–10% (*DNAI1*[12,13]) of total cases. The other genes are so far only associated with single or rare PCD cases; therefore, the genetic basis of at least 60% of PCD cases is not yet known. Several additional PCD loci have been mapped, including those on chromosomes

[1]General and Adolescent Paediatric Unit, University College London (UCL) Institute of Child Health, Rayne Building, 5 University Street, London WC1E 6JJ, UK; [2]Nephro-Urology Unit, University College London (UCL) Institute of Child Health, 30 Guilford Street, London WC1N 1EH, UK; [3]Division of Child Health, Department of Infection, Immunity, and Inflammation, University of Leicester, Robert Kilpatrick Clinical Sciences Building, Leicester Royal Infirmary, Leicester LE2 7LX, UK; [4]Neural Development Unit, University College London (UCL) Institute of Child Health, 30 Guilford Street, London WC1N 1EH, UK; [5]Institute for Science and Technology in Medicine, School of Medicine, Keele University, Thornburrow Drive, Hartshill, Stoke-on-Trent ST4 7QB, UK; [6]Department of Cell and Development Biology, University College London, Gower Street, London WC1E 6BT, UK; [7]Department of Paediatric Respiratory Medicine, Great Ormond Street Hospital for Children NHS Trust, London WC1N 3JH, UK; [8]Section of Ophthalmology and Neurosciences, Wellcome Trust Brenner Building, Leeds Institute of Molecular Medicine, St James's University Hospital, Beckett Street, Leeds LS9 7TF, UK; [9]Human Diversity Unit, Department of Molecular and Human Genetics, College of Medicine, Florida International University, 11200 SW 8th St., Miami, FL 33199, USA; [10]Department of Paediatric Respiratory Medicine, Royal Brompton and Harefield NHS Trust, Sydney Street, London SW3 6NP, UK; [11]Genetics Institute, Assaf Harofeh Medical Center, Zerifin 70300 and the Sackler School of Medicine, Tel Aviv University, 69978 Tel Aviv, Israel; [12]Algal Research Group, Institute of Structural and Molecular Biology, University College London, Gower Street, London WC1E 6BT, UK; [13]Molecular Medicine Unit, University College London (UCL) Institute of Child Health, 30 Guilford Street, London WC1N 1EH, UK
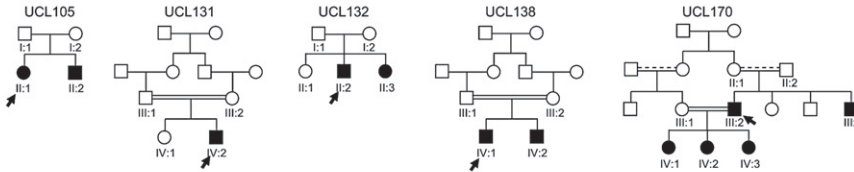*Correspondence: h.mitchison@ich.ucl.ac.uk

A

Bedouin families
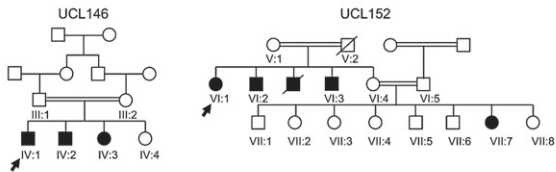
Transposition defect families

B

C

D
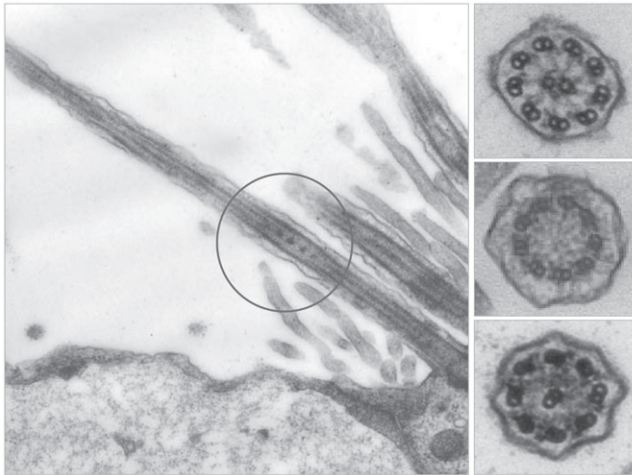
SNP	Position	cM	UCL138		UCL131		UCL132		UCL170	
						Family ID				
rs6929015	104215377	106.85	A	G	A	A	A	G	G	G
rs860933	104609135	107.06	G	G	A	A	A	G	G	G
rs201204	104842863	107.20	G	G	G	G	G	G	A	A
rs880177	105957405	108.08	A	G	A	A	G	G	A	G
rs9386461	106176614	108.30	A	G	G	G	G	G	A	G
rs1475270	106794072	109.56	A	G	A	A	A	A	A	A
rs1665914	107436099	110.86	A	G	G	G	A	A	A	A
rs2050042	108415352	112.16	A	A	C	C	A	A	A	A
rs217532	108628006	112.45	A	A	C	C	A	A	A	A
rs1260658	109526918	113.49	A	A	G	G	G	G	G	G
rs351755	109644766	113.61	A	A	G	G	G	G	G	G
rs736830	109819992	113.79	C	C	C	C	C	C	C	C
rs1046943	109890634	113.86	G	G	G	G	G	G	G	G
rs781499	111367616	115.34	G	G	G	G	A	A	A	A
rs1022092	111533979	115.51	G	G	G	G	A	A	A	A
rs1158747	112607343	116.35	A	A	A	A	C	C	C	C
rs3851197	113772693	117.57	G	G	G	G	G	G	A	A
rs1565528	113776568	117.57	A	A	A	A	A	A	A	A
rs1491074	113790603	117.58	G	G	G	G	G	G	G	G
rs1033391	113866756	117.59	G	G	G	G	G	G	G	G
rs773676	114155885	117.71	A	A	A	A	A	A	A	A
rs2030926	114173820	117.71	G	G	G	G	G	G	G	G
rs963884	114236941	117.74	A	A	A	A	A	A	A	A
rs548388	114342082	117.75	A	A	A	A	A	A	A	A
rs1415428	114798204	117.76	A	A	A	A	A	A	A	A
rs7759765	115886352	117.97	G	G	G	G	G	G	G	G
rs1041883	116796071	118.39	A	A	A	A	A	A	A	A
rs9398436	116920626	118.44	A	A	A	A	A	A	A	A
RSPH4A										
rs544047	117715011	118.79	G	G	G	G	G	G	G	G
rs1321807	117791685	118.82	G	G	G	G	G	G	G	G
rs2243379	117831155	118.84	A	A	A	A	C	C	A	A
rs1407184	117840410	118.84	A	A	A	A	G	G	A	A
rs1321813	117934984	118.88	A	A	A	A	C	C	A	A
rs210617	117966751	118.90	A	A	A	A	A	A	A	A
rs1541317	118130009	118.97	C	C	C	C	C	C	C	C
rs1012509	119549906	119.55	A	A	A	A	A	A	G	G
rs7758258	119874817	119.71	A	A	A	A	A	A	C	C
rs937091	120236615	119.83	C	C	C	C	C	C	A	A
rs1486198	120848386	119.83	A	A	A	A	A	A	G	G
rs10456936	121323877	119.91	A	A	A	A	C	C	A	A
rs763075	122253219	120.49	A	A	A	A	A	A	A	A
rs1563512	122521445	120.96	A	A	A	A	A	A	A	A
rs873460	123766181	123.13	G	G	G	G	G	G	G	G
rs1321084	123944240	123.44	C	C	C	C	C	C	A	A
rs941815	123962271	123.47	G	G	G	G	G	G	G	G
rs1407529	124726881	124.80	G	G	G	G	G	G	G	G
rs659491	124870435	125.05	A	A	A	A	A	G	G	G
rs781739	125274032	125.52	A	A	A	A	A	A	A	A
rs911966	125433792	125.52	A	C	C	C	A	A	C	C
rs524394	125573809	125.71	C	A	A	A	C	C	C	C
rs1569741	126425169	126.86	A	G	G	G	G	G	G	G
rs1340952	126993203	127.23	A	A	A	A	A	A	A	G
rs1538956	127005719	127.23	A	A	A	A	A	A	A	C
rs1022573	127096607	127.26	C	C	C	C	C	C	A	C
rs988693	127339126	127.33	A	G	G	G	A	A	A	G
rs1543432	127739711	127.46	G	G	G	G	A	A	A	G
rs482607	129027553	128.21	G	A	G	G	G	G	G	G
rs1894641	130062643	129.27	A	A	G	G	A	G	G	G
rs2007339	131387357	130.64	G	G	G	G	G	G	G	G
rs942150	131744986	130.72	A	C	C	C	A	A	C	C
rs1033540	131778995	130.74	A	G	A	A	A	G	G	G
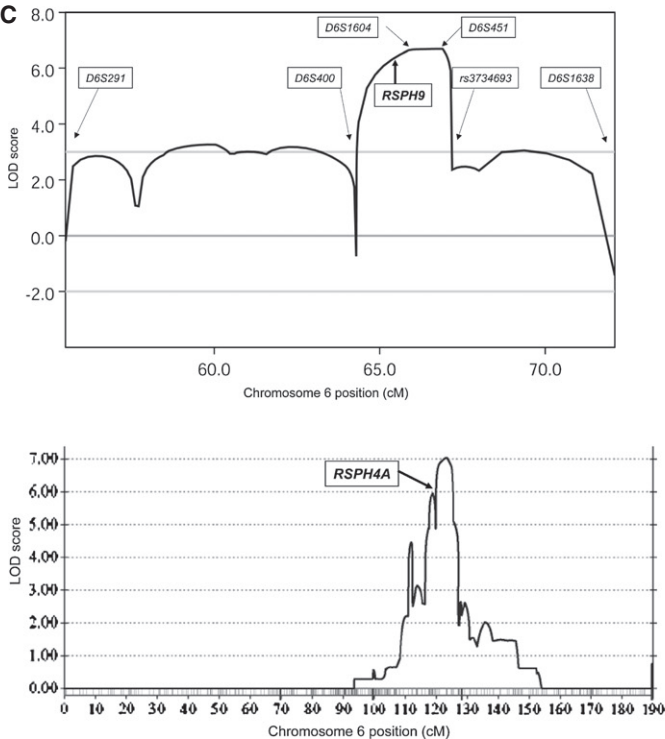
19q13,[14] 16p12,[3] 15q13-q15,[3] and 15q24-q25,[15] but these genes remain to be isolated (reviewed by Geremek and Witt[16]). The possibility of involvement of PCD genes in sensory- and retinal-cilia functions is suggested by reports of syndromic forms, similar to PCD, that have motile-cilia dysfunction and additional features, including retinitis pigmentosa,[17] polycystic kidney disease,[18] and mental retardation.[19]

Patients with ultrastructural abnormalities affecting the central microtubular pair represent a well-recognized subgroup in whom laterality defects have not been observed.[20] This is assumed to reflect the 9+0 ultrastructure of nodal cilia, which may be unchanged by mutations affecting a structural element that they do not possess (in most species). Using two distinct family groups affected by PCD associated with central-microtubular-pair defects, we performed SNP-based whole-genome linkage analysis to identify the disease-causing genes.

Subjects and Methods

Families, Clinical Information, and Controls

Informed consent was obtained from patients and family members in accordance with protocols approved by the University College London Hospital NHS Trust ethical committee and collaborating institutions. The diagnosis of PCD was based on the exclusion of cystic fibrosis, immunodeficiency, and tuberculosis and the presentation of classic clinical features. These features included the following: reduced exercise tolerance; chronic wet cough; recurrent respiratory infections; nasal symptoms, including rhinorrhea, rhinitis, nasal blockage, and sinusitis; in addition to glue ear and consequent hearing problems. Bronchiectasis also occurred. Low weight and short stature were noted in the Bedouin and Pakistani families.

The pedigrees are presented in Figure 1A. Family UCL146 from the United Arab Emirates (UAE) was previously reported, showing one patient with a collapsed lower-left pulmonary lobe.[20] The family originated from the Bedouin Bani Tameem tribe, and the parents are first cousins. There is an unusual intermittent loss of the central pair in this family, confirmed by longitudinal-section electron microscopy in all three affected children, such that cilia cross-sections show a small proportion with 9+0 structure. Family UCL152 from Israel is also Bedouin, with multiple consanguineous unions within the extended pedigree. Transmission electron microscopy (TEM) performed on one affected member showed a normal axoneme ultrastructure. Family UCL152 was included in the study despite an apparently normal ultrastructure because of respiratory symptoms consistent with a diagnosis of PCD, as described above, and dysmotility of the respiratory cilia, as described below. Furthermore, dysmotile sperm was also reported in two males, and one female required in vitro fertilization treatment as a result of subfertility.

Family UCL105 is a nonconsanguineous UK-Northern European family. Families UCL131, UCL132, UCL138, and UCL170 are all of Pakistani origin, now residing in the north of England. The parents in all of these families except family UCL132 are first cousins; any consanguinity in family UCL132 was not known to the family. TEM in affected children from all five families showed a classic ciliary transposition defect indicative of complete central-pair loss, as described in Stannard et al.[20]

Cilia-motility studies on nasal-biopsy samples collected from affected patients in all seven families showed an abnormal circular movement with a close to normal beat velocity, except for UCL152, which was recorded as having "abnormal motility." Visualizing a circular pattern is dependent on viewing at the correct orientation, and this can account for some variability in recording.

Control DNA consisted of UK-Northern European samples from panels 1 and 2 of the European Collection

---

Figure 1. Central-Pair Agenesis in PCD Patients and Linkage Analysis

(A) PCD central-pair-defect pedigrees. Black indicates affected; double line indicates consanguineous union, with a dashed upper line if the exact degree of relatedness is unknown; arrow indicates proband.

(B) Transmission electron micrographs of nasal ciliary epithelium from individuals with a central-pair defect. Left panel, Bedouin UCL146 IV:1 longitudinal section with intermittent central-pair loss, confirming the previous report[20] of 9+2 (normal) and 9+0 cross-sections. Right panels, cross-sections from UK-Pakistani UCL170 IV:1, indicative of complete central-pair loss (transposition defect), showing 9+2 (upper panel), 9+0 (middle panel), or 8+1 (lower panel) ultrastructure.

(C) Linkage mapping of families with central-pair defects, to two loci, on chromosome 6p21.1 and 6q22.1. Upper panel, multipoint MERLIN linkage analysis of UCL146 and UCL152 on 6p21.1 across *D6S291–D6S1638*, with the use of information from Illumina and deCODE scans and in-house microsatellite genotyping. The overlapping shared region of IBD from *D6S400* to *rs3734693* is reflected by a significant multipoint LOD score > 3, which rises to a peak of 6.7 across *D6S1604–D6S451*. The location of *RSPH9* is shown. Lower panel, multipoint GENEHUNTER linkage analysis of families with transposition defect on 6q22.1 across chromosome 6, with the use of Illumina scan information. The location of *RSPH4A* is shown, located centromeric to the peak homogeneity LOD score of 7.0, which was generated across markers *rs873460–rs941815*.

(D) Identical-by-descent homozygosity and founder effect in *RSPH4A* families. Chromosome 6q22.1 disease-chromosome haplotypes for each of the four UK-Pakistani families are shown, displaying extended homozygosity across the *RSPH4A* locus. Bold, black lines and boxes indicate the linked region in each pedigree, defined by recombination events or loss of homozygosity. The minimal critical region containing *RSPH4A* is *rs2030926–rs937091* (defined by recombinations in UCL138). Homozygous allele sharing occurs among affected individuals (gray shading), with a putative minimal common ancestral haplotype spanning the *RSPH4A* gene, across markers *rs1158747–rs2243379* (light gray).

of Cell Cultures (ECACC) Human Random Control Collection, anonymized UK-West Midlands Pakistani individuals (UK-Pakistani), Bedouin samples purchased from the National Laboratory for the Genetics of Israeli populations, unrelated UAE males previously reported,[21] and additional unrelated members of other pedigrees (13 Pakistani and 26 Arabic), collected for mapping and polymorphism studies.

Linkage Analysis and Autozygosity Mapping

Genome-wide linkage analysis was performed in all families with the 0.64 cM density Illumina Linkage IVb 6008 SNP panel and in family UCL152 with the 8 cM density deCODE 500 microsatellite panel. SNP genotyping was performed at the Turku Centre for Biotechnology, Finland or at deCODE Genetics, Reykjavik, Iceland. Multipoint linkage analysis with the use of MERLIN 1.0.1 (within easy-LINKAGE)[22,23] or GENEHUNTER 2.1r5[24] was performed under the assumption of autosomal-recessive inheritance, 0.9 penetrance, 0.007 disease-allele frequency, and 0.00001 phenocopy rate, with allele frequencies set according to Illumina and deCODE map information.

Candidate-Gene Identification and Sequence and Protein Analysis

All known and predicted genes were identified at the *RSPH9* locus with the UCSC, NCBI, and Ensembl genome browsers, then prioritized for sequencing with the assumption that PCD genes should be conserved in distantly related ciliated organisms but absent in nonciliated organisms. For identification of this class of gene, a protocol of serial BLAST searches[25] was developed to interrogate draft genome sequences of twelve organisms, three nonciliated (*A.thaliana*, *S.pombe*, *S.cerevisiae*) and nine ciliated (*C.reinhardtii* genome, proteome,[26] and deflagellation data set;[27] *T. brucei* proteome;[28] *T. brucei*/*L.major* combined genomes;[29] *C. intestinalis* genome; *T. thermophilia* genome; *C. elegans* proteome (sensory cilia only); and a *Foxj1* mouse ciliogenesis microarray of genes downregulated in this cilia-less mouse [S. Brody, Washington University, personal communication]). The process of database formatting, local BLAST searching, and data parsing was automated with a custom perl script (Blast2 matrix; available on request from R.D.E.: r.d.emes@hfac.keele.ac.uk). For this experiment, significant alignment results were determined with the use of an E value of $\leq 10^{-5}$ cutoff. The C6orf206 (RSPH9) protein was conserved in eight ciliate databases but not in *C.elegans* (sensory cilia only) or the three nonciliate databases.

Three prioritized positional candidate genes on chromosome 6p21.1, *TBCC* (MIM 602971), *KNSL8*, and *C6orf206* (initially annotated as a mitochondrial ribosomal gene and since renamed as *RSPH9*), in addition to the *RSPH4A* gene on chromosome 6q22.1, were sequenced with genomic DNA from linked patients and primers designed to span the coding exons and splice sites. Primer sequences for *RSPH9* and *RSPH4A* are shown in Table S1 (available online), and all other primer sequences are available on request. Sequence alignments to analyze conservation of mutated residues were generated using ClustalW and Boxshade. Protein domain analysis was conducted using SMART, PFAM, Genthreader and Scansite prediction tools.

Restriction-digest tests (*RSPH9* p.Lys268 del, MboII [shown in Figure S3]; *RSPH4A* p.Gln154X, BsmAI; p.Pro87Ser, SacII; p.Gln109X, BspCNI) or sequencing (RSPH4A p.Arg490X) confirmed the inheritance pattern of all mutations in all extended kindreds.

In Situ Hybridization

The *Rsp9* probe corresponded to the area from nt 317 in exon 2 to nt 837 in exon 5, amplified from mouse Riken cDNA clone 1700027N10 (RZPD German Resource Centre) with primers 5′-TGGTGAGTGGCCGTTTCAT-3′ and 5′-CCATGTTCTTCTCTCCTGTGC-3′, and the product was cloned into pCR4 by TOPO-TA cloning (Invitrogen). The mouse *Dnah5* probe in pBluescript SKII[+30] was kindly provided by H. Omran, University Hospital Freiburg. Sense and antisense digoxygenin-labeled riboprobes were prepared with the use of a digoxigenin RNA-labeling kit (Roche) and purified on Chroma Spin-100 columns (BD Biosciences), prior to in situ hybridization on whole-mount embryos or 7 μm paraffin-wax sections. Randomly bred CD1 mice served as a source of mouse embryos and fetuses. Litters were generated by timed matings, and the day that a copulation plug was found was designated embryonic day 0.5 (E0.5). Embryos were collected at E7.5, E18.5, and E19.5. Whole-mount in situ hybridization was performed as described previously.[31] In situ hybridization on sections was performed as described previously[32] and photographed with an MZFLIII, DC500 imaging system (Leica). Sense-strand controls yielded no specific hybridization signal.

Zebrafish Morpholino Injections

Morpholinos (MOs) were designed against the splice-donor sites of zebrafish *rsph9* exon 2 (MOex2: 5′-GGTGTAAGGCTTTTACCGTGACCTC-3′) and exon 3 (MOex3: 5′-GCTGTAAGTATACCTCCAAAGCTTC-3′) (GeneTools). One- to two-cell-stage embryos were injected with 6.25 ng of MO in Danieau buffer (5 mM HEPES pH7.6, 58 mM NaCl, 0.7 mM KCl, 0.4 mM MgSO$_4$, 0.6 mMCa(NO$_3$)$_2$). Green fluorescent protein (GFP) mRNA was coinjected for determining correct MO distribution. Siblings from the same pool as the MO-injected embryos served as negative controls. Effective doses were determined for each MO with the use of a concentration in which MO-injected embryos developed normally. Higher doses causing detectable detrimental effects on development were not pursued further.

Primers 5′-AGCGAATAGATCGAGATGGAC-3′ and 5′-TGGAGATTGTGTCGCTGAAG-3′ were used for confirming missplicing, by RT-PCR, of RNA isolated with TRIzol (Invitrogen) from ten control or MO-injected embryos, at 24 and 72 hr postfertilization (hpf). PCR products were gel purified (Invitrogen) and sequenced to reveal missplicing events.

For motility studies, 7–9 control and MO-injected embryos at 72 hpf, confirmed as alive by observation of heartbeat beforehand, were analyzed individually under glass coverslips. Olfactory-pit cilia were viewed under a water-immersion objective lens (×50) on an inverted Nikon Diaphot microscope in a humidified (80%) and temperature-controlled (28°C) chamber. High-speed (500 frames per second [fps]) video sequences of the zebrafish olfactory pits were captured (Trouble-shooter 500, Lake Image systems, UK). The stored sequences were then replayed in slow motion (Midas 2.0 player, Xcitex) and the cilia beat frequency (CBF) was calculated as previously described,[33] with the use of the following formula: fps (500) / number of frames elapsed for five beat cycles × beat cycles counted (5) = CBF (Hz). The immotility index (II) and dysmotility index (DI) were determined by a count of the number of static (II) or dysmotile (DI; abnormal movement + static) cilia as a percentage of the total number present in the video sequences. The mean ± SEM was calculated for 7–9 embryos, and data were tested by one-way ANOVA, with individual data sets compared by an unpaired Student's t test with Bonferroni correction for repeated-measures.

Zebrafish Phenotype Rescue
Full-length mouse *Rsph9* mRNA was subcloned into pßUT3 vector, and mRNA was transcribed with the mMessage machine kit (Ambion) and T3 polymerase, then titrated for determination of the maximum effective injection dose. One-cell-stage embryos were coinjected with 150 pg mRNA and 6.25 ng of MO via methods described above, and olfactory-cilia movement was assessed at 72 hpf as described above. The controls were WT and MO-treated embryos.

Chlamydomonas Strains and Maintenance
WT (CC-1732 and *cw*15), *pf17* parental (CC-1035), and progeny (CC-1332, CC-1143, CC-2645, and CC-262) strains were obtained from the *Chlamydomonas* Genetics Center (see Web Resources). Cells were grown and expanded via standard protocols in Tris-acetate phosphate (TAP) medium,[34] under light (~45 µE/m²/s), at 25°C.

Identification of *Chlamydomonas* *pf17*-Strain Mutation
The precise genetic lesion in *Chlamydomonas* mutant strain *pf17* had not previously been identified. The five coding exons, intron-exon boundaries, and 5′ and 3′ UTRs of *RSP9* were sequenced in genomic DNA isolated, via a method adapted from Goldschmidt-Clermont et al.,[35] from WT *Chlamydomonas* and mutant *pf17*. This revealed a single-bp deletion in exon 2 (c.131delG) present in *pf17* but not in the WT, predicting a premature stop codon after Ser45 in the 269 residue protein. This change abolishes a *BspEI* restriction site, and we confirmed that the mutation causes the paralyzed flagella phenotype and had not arisen since original isolation of *pf17*, by *BspEI*

restriction digest of a 1.1 kb exon 2 PCR product, amplified with primers 5′-CGCAGCTCACTTATCTCTTCCT-3′ and 5′-AGCACACGCCTCATCCAATAG-3′, from genomic DNA isolated from the WT, the original *pf17* mutant strain CC-1035, and its four *pf17* progeny strains: CC-1332, CC-1143, CC-2645 and CC-262. The c.131delG mutation identified in mutant *pf17* was present in the original *pf17* and all progeny strains, but not in the WT control (data not shown).

Chlamydomonas RSP9 Vectors
Transformation vectors for creating the *pf17*-T and *pf17*-Tmut strains were made as follows: The WT genomic *RSP9* gene was amplified from genomic DNA with pFusion *Taq* (Invitrogen) and PCR primers P1 (5′-AGATTCCACA CCTCACGGATAC-3′) and P2 (5′-ACCAGTCAAACTTTCG AACCAG-3′) to include the 5′ and 3′ UTR and approximately 400 bp of the upstream sequence incorporating the tub-box sequence motif known to enhance transcription after deflagellation,[36] then cloned into pBluescript SKII⁻. A mutated *RSP9* was created through introduction of a 3 bp deletion into this WT DNA construct, mimicking the human c.801_803delGAA; p.Lys268del mutation. The resulting mutation in *Chlamydomonas RSP9*, a deletion of the homologous residue, is c.780-783delCGC; p.Arg261del (Figure S2A). This was done with the use of a primer with the relevant 3 bp missing and a *BmgBI* restriction site at the 5′ end (P3: 5′-CGAGCTGACGTGGGGCAGCCTGT ACGTGGGCGACGGCCTGAACAACGACC-3′) and the use of a reverse primer (P4: 5′-GTATGTTGTGTGGAATTGT GAGCGG-3′) complementary to pBluescript, downstream of a unique NotI site. The pBluescript WT *RSP9* construct was amplified with P3-P4, and the product was subcloned into pCR4 by TOPO-TA cloning (Invitrogen) and then excised by BmgBI and NotI double digestion. pBluescript WT *RSP9* was separately BmgBI and NotI double digested for elimination of the WT *RSP9* insert, then these DNAs were ligated, creating a pBluescript plasmid containing mutated *RSP9*.

Chlamydomonas Transformation
Immotile *pf17* (CC-1035) mutant *Chlamydomonas* were transformed with the WT or mutated *RSP9* vectors, with the use of a modified protocol from Kindle.[37] *pf17* was first backcrossed with cell-wall-less mutant *cw15*, for ease of transformation. Backcrossed *pf17* cultures (as well as cell-wall-less *cw15* control cultures) were then used. Cells were resuspended to 2×10^8 cells/ml, and 300 µl was transferred to 5 ml tubes containing ~0.3 g of 0.4 mm diameter washed glass beads (BDH). 1 µg plasmid DNA and 4 µg plasmid pSI103, which confers paramomycin antibiotic resistance for selection of transformant colonies, were added together, and the mixture was vortexed for 15 s and grown overnight with slow shaking to allow for recovery and gene expression. Cells were plated on TAP 2% agar supplemented with 20 µg/ml paramomycin and inverted in the light at 22°C. Transformed cell-wall-less

pf17 colonies were visible after 7–10 days and were then selected by viewing 100 colonies of each and monitoring them for rescued motility. The *pf17* strain transformed with WT *RSP9* was called *pf17*-T, and *pf17* transformed with mutant *RSP9* was called *pf17*-Tmut.

The correct incorporation of WT and mutant *RSP9* constructs into the genetic material of these transformed strains was confirmed in genomic DNA by restriction digest, making use of the *BspEI* site destroyed by the original *pf17 RSP9* c.131delG mutation. In addition, the c.780_783delCGC mutation mimicking that of human *RSPH9* patients destroys an *FspI* site. *BspEI* and *FspI* digests showed that the control *cw15* strain carried WT *RSP9*, the *pf17*-T strain carried both WT and c.131delG *RSP9*, and the *pf17*-Tmut strain carried no WT *RSP9* but did carry c.131delG and c.780_783delCGC mutated *RSP9*. Thus, the WT and mutant *RSP9* constructs had incorporated correctly into the genetic material of *pf17*-T and *pf17*-Tmut.

Chlamydomonas-Motility Analysis

Cell-wall-less *cw15*, *pf17*, *pf17*-T, and *pf17*-Tmut were picked into TAP medium, grown overnight, and analyzed under a water-immersion objective lens (×50) on an inverted Nikon Diaphot microscope in a humidified (80%) and temperature-controlled (30°C) chamber. High-speed (500 fps) video sequences were captured (Troubleshooter 500, Lake Image systems, UK), and the stored sequences were replayed in slow motion (Midas 2.0 player, Xcitex) for measuring flagella beat frequency (FBF) using the formula published by Chilvers et al.[44]: fps (500) / number of frames elapsed for five beat cycles × beat cycles counted (5) = FBF (Hz). *Chlamydomonas* flagella do not beat with a planar motion as cilia do but, rather, can change the beat direction to facilitate directional movement, and motility was too variable to allow for calculation of a meaningful DI as was performed for zebrafish; therefore, only an II was calculated, when the beat pattern was symmetrical. This was determined by a count of the number of static flagella as a percentage of the total number present in the video sequences. The means ± SEM were calculated for 21 (*cw15*), 26 (*pf17*), 20 (*pf17*-T), and 21 (*pf17*-Tmut) embryos for FBF and for 10 (*cw15*), 5 (*pf17*), 7 (*pf17*-T), and 10 (*pf17*-Tmut) embryos for II. Data were tested by one-way ANOVA, and individual data sets were compared with the use of an unpaired Student's t test with Bonferroni correction for repeated measures.

Results

We undertook genome-wide linkage analysis and subsequent positional-candidate-gene analysis in seven PCD families with central-microtubular-pair defects: two Bedouin, four UK-Pakistani and one UK-Northern European (Figure 1A). Five of the families were consanguineous.

No patients displayed laterality defects. For those in whom ciliary movement was studied, the ciliary beat frequency was within the normal range. However, the beat pattern was recorded as being circular rather than having the normal forward and backward planar motion,[33] for all seven families except one Bedouin family, in which the beat pattern was recorded as "abnormal motility" (detailed in Subjects and Methods). One of the two Bedouin families, UCL146, had an unusual intermittent absence of the central pair, resulting in cilia cross-sections with both a 9+2 and a 9+0 ultrastructure[20] (Figure 1B), and the second family, UCL152, had an apparently normal ultrastructure. The other five families, UCL105, UCL131, UCL132, UCL138, and UCL170, had a classic "transposition" defect, consisting of complete absence of the central pair and ciliary transposition. As previously described,[20] in this defect, a proportion of cilia cross-sections have an absent central pair (9+0) and a proportion have an 8+1 arrangement, in which the central pair is absent and one peripheral microtubule doublet with attached dynein arms is transposed to the center (Figure 1B).

Identical-by-descent (IBD) regions of homozygosity shared among the affected individuals were identified in the two family groups. The full results of the whole-genome linkage scan are shown in Figure S1. For the two Bedouin families, a 4.8 Mb region in UCL146, between *rs1738240* and *rs945131*, overlapped with a 10.8 Mb region in UCL152, between *D6S291* and *D6S452* (not shown). Higher-resolution genotyping using known or in-house-designed microsatellites defined a common 1.9 Mb critical region of IBD between markers *D6S400* and *rs3734693* on chromosome 6p21.1, with a peak multipoint LOD score of 6.7 across *D6S1604–D6S451* (Figure 1C). Across this 1.9 Mb IBD region, the two families shared alleles at only two microsatellite markers, located either side of *RSPH9*, such that any linkage disequilibrium between the families is small (0.6 Mb maximum) (not shown).

All five transposition families were linked, with the use of only Illumina data, without additional genotyping, to a single 6.7 Mb region from *rs2030926* to *rs937091* on chromosome 6q22.1, defined by recombination events in family UCL138 (Figures 1C and 1D). There was a peak multipoint LOD score of 7.0 across *rs873460–rs941815*. No other genomic region was significant for linkage (Figure S1). The four UK-Pakistani families shared an IBD region and a common 5.2 Mb haplotype across markers *rs1158747–rs2243379*, suggesting a founder effect. This was shared among all ten affected individuals, including those of UCL132, a family that appears to have previously unknown consanguinity and ancestral sharing with the other three UK-Pakistani families (Figure 1D). The UK-Northern European family (UCL105) was consistent for linkage across the 57 Mb (*rs1014976–rs1385732*) spanning this region but had no significant marker homozygosity or allele sharing with the Pakistani families (not shown).

The linked region in the two Bedouin families harbored the positional candidate gene *RSPH9*. A homozygous 3 bp
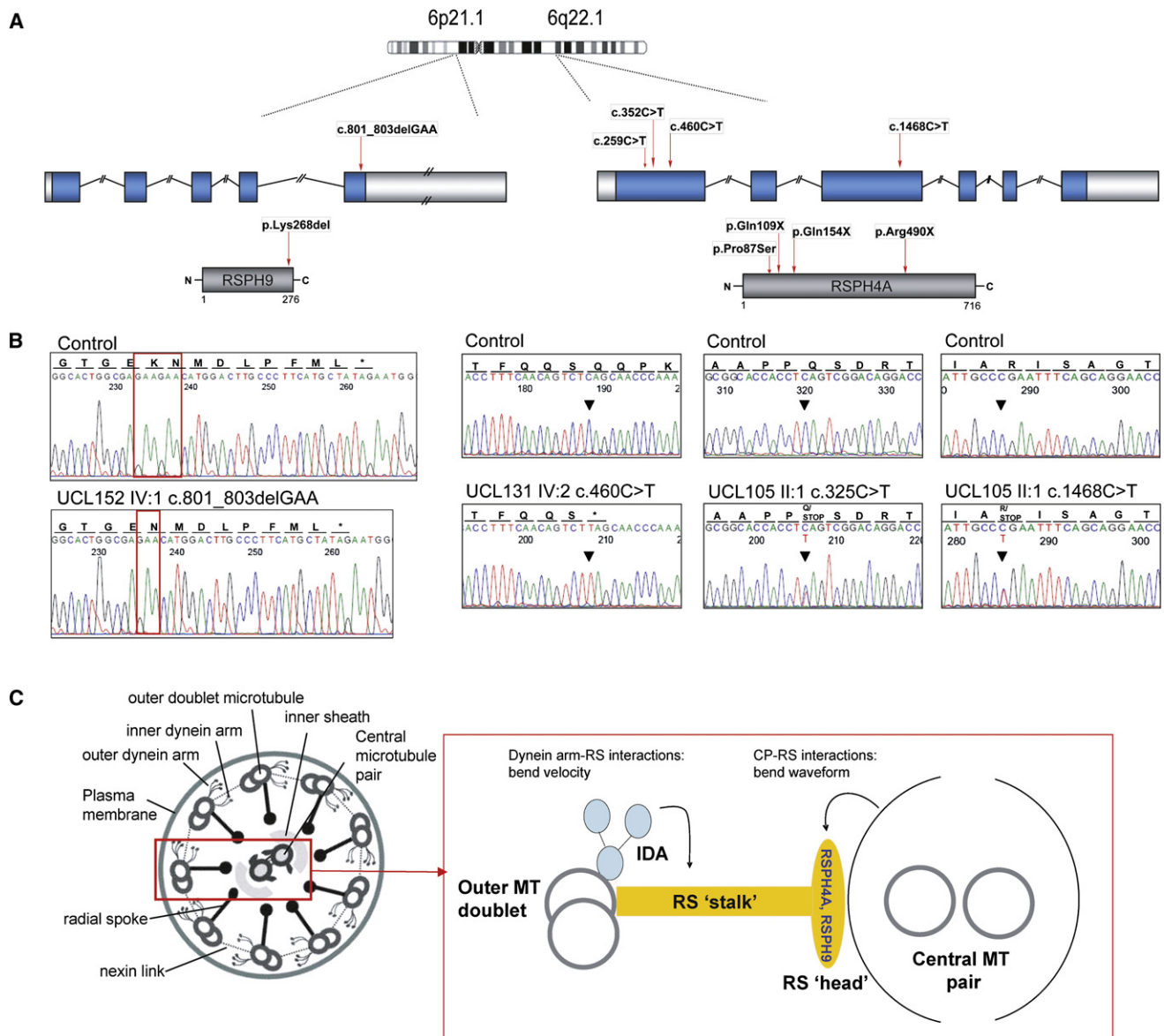
Figure 2. RSPH9 and RSPH4A Mutations
(A) Chromosome 6 location of RSPH9 (left) and RSPH4A (right), their genomic structure showing the 5′ and 3′ UTRs (white), introns and exons (blue), their derived proteins (grey), and mutations.
(B) Electropherograms indicate the normal sequence (top traces) and mutations (bottom traces).
(C) "9+2" cilia axoneme model (cross-section) with putative RSPH9 and RSPH4A location, based on *Chlamydomonas* homology. Abbreviations are as follows: CP, central microtubular pair; RS, radial spoke; IDA, inner dynein arm; MT, microtubule.

deletion (c.801_803delGAA) was identified in all seven affected Bedouin individuals, predicting in-frame loss of the C-terminal Lys268 (p.Lys268 del) (Figures 2A and 2B). This residue is largely conserved across distant phyla (Figure S2A). Screening of population-matched controls revealed that this change was not carried on 126 Bedouin and Arabic control chromosomes. However, screening of chromosomes from a collection of 160 unrelated control UAE males[21] showed that three individuals were heterozygous for this amino acid deletion, a result that was not regarded as surprising given the high incidence of consanguineous unions in the culturally isolated UAE popula-

tion.[38] The overall frequency of this change in all of the control chromosomes screened was 0.7%. These findings therefore suggest that RSPH9 mutations probably cause PCD.

The linked region in the five families with a transposition defect harbored the positional candidate gene RSPH4A, also located within the region spanned by the ancestral UK-Pakistani haplotype (Figure 1D). Four C-to-T transition-sequence variants were identified (Figures 2A and 2B). All ten affected UK-Pakistani individuals were homozygous for a nonsense mutation, p.Gln154X (c.460C→T), accompanied by a second upstream missense variant, p.Pro87Ser (c.259C→T). Patients in the Northern
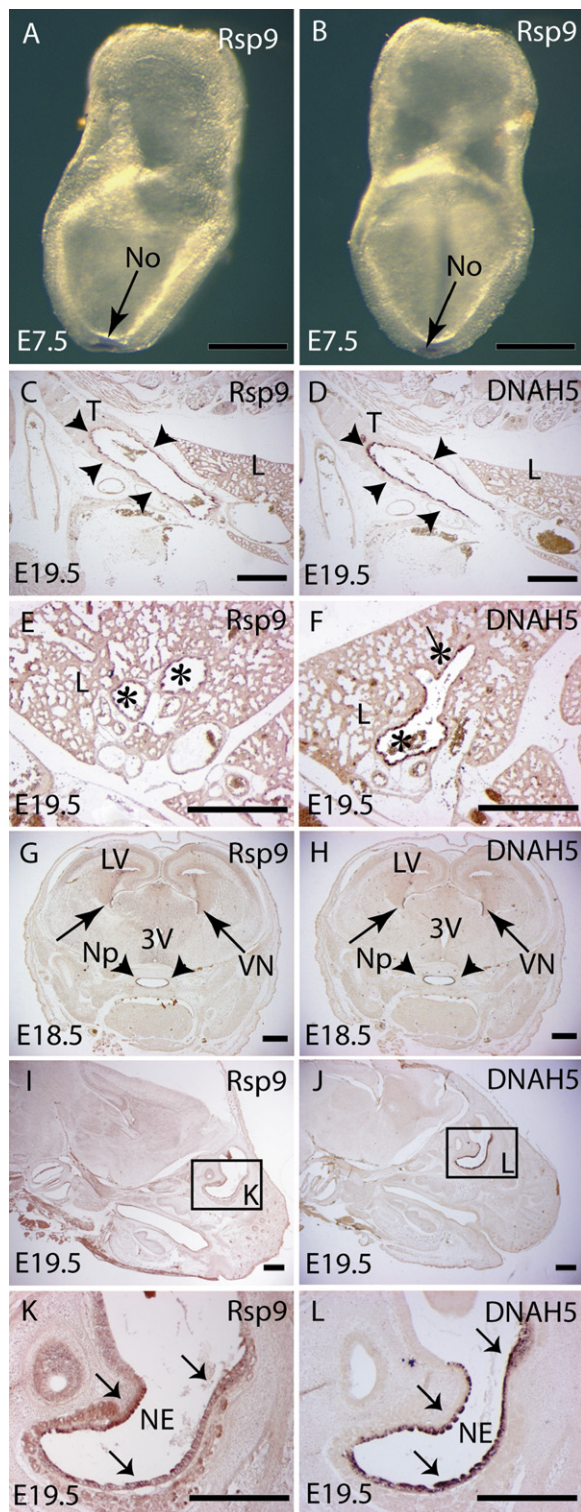
Figure 3. Expression of *Rsph9* in the Node and Ciliated Epithelia

Whole-mount in situ hybridization of *Rsph9* reveals specific expression in the node (No) of E7.5 mouse embryos (arrow); side (A) and anterior (B) views. Expression of *Rsph9* (C, E, G, I, K) and *Dnah5* (D, F, H, J, L) detected by in situ hybridization on sagittal (C–F and I–L) and coronal (G and H) sections at E18.5 (G and H) and E19.5 (C–F and I–L). Similar expression of both genes was detected in the epithelia lining the trachea (T) (arrow-heads in C and D), the bronchi (asterisks in E and F), and the naso-pharynx (Np) and neuroepithelium of the lateral ventricles (VN) (G and H). Expression was also prominent in the olfactory epithelium (I and J, magnified in K and L). Abbreviations are as follows: L, lung; LV, lateral ventricle; NE, nasal epithelium; 3V, third ventricle. Scale bar represents 500 μm.

European family UCL105 were compound heterozygous for nonsense mutations pGln109X (c.325C→T) and p.Arg490X (c.1468C→T). Cosegregation of all mutations with the disease status in all extended kindreds was confirmed and was found to be in accordance with haplo-types (Figure S3, Subjects and Methods). Screening of pop-ulation-matched controls showed that they did not carry any of the identified *RSPH4A* mutations. These controls comprised 154 UK-Pakistani chromosomes screened for the p.Pro87Ser and p.Gln154X mutations; 170 and 354 UK-Northern European control chromosomes were also screened for the p.Pro87Ser and p.Gln154X mutations, respectively. In addition, 348 and 368 UK-Northern Euro-pean chromosomes were screened for the p.Gln109X and p.Arg490X mutations, respectively.

Both *RSPH9* and *RSPH4A* are predicted to encode radial spoke head proteins (Figure 2C), on the basis of homology with proteins of known function in the biflagellate alga *Chlamydomonas reinhardtii* and other ciliates.[39] The RSPH9 protein was identified as 28% identical to biflagel-late alga *Chlamydomonas reinhardtii* radial spoke head 9 (RSP9) protein.[39] The RSPH4A protein was identified as 31% and 30% identical, respectively, to two similar *Chla-mydomonas* proteins, RSP4 and RSP6 (Figure S2B).

Radial spokes are regularly spaced along cilia, sperm, and flagella axonemes and have a multisubunit "stalk" and "head" that form a signal-transduction scaffold between the central pair and the dynein arms (Figure 2C). Available evidence suggests that they regulate dynein-induced movement and govern cilia and flagella waveform. Central pair–radial spoke interactions determine bend direction and shape (waveform), whereas radial spoke–inner dynein arm interactions influence velocity.[39–41]

Further investigation of orthologs of *RSPH9* were under-taken in three model organisms: mouse, zebrafish (*Danio rerio*), and *Chlamydomonas*, for determination of the patho-genic potential of the in-frame Lys268del change. We determined the tissue distribution of *Rsph9* gene expression in mouse. In situ hybridization showed specific expression in nasal, lung, trachea, and brain ventricle epithelium at E18.5–19.5 and at the embryonic node at E7.5. This was a similar pattern to that of *Dnah5*,[6,30] which is restricted to regions where motile cilia are located (Figure 3).

We investigated *rsph9* knockdown in zebrafish. Two different *rsph9* splice-site MOs directed against the exon 2 (MOex2) and exon 3 (MOex3) splice-donor sites were used for disruption of gene expression (Figure S4). Both gave a dose-dependent phenotype of dysmotile olfactory-pit cilia with a normal beat frequency but an ineffective circular
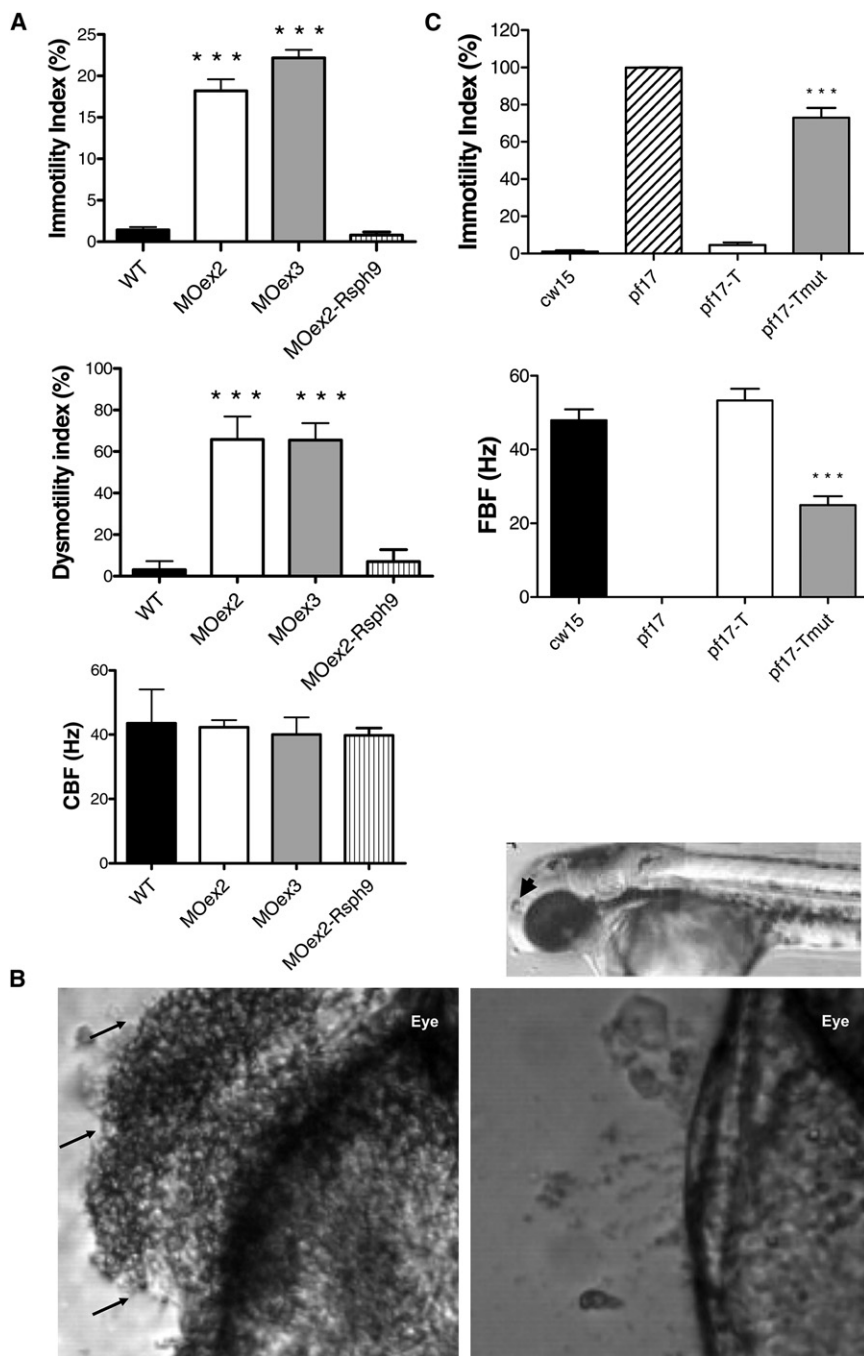
Figure 4. Loss of Zebrafish and *Chlamydomonas* RSPH9 Gene Function, Causing Dysmotility of Cilia and Flagella

(A) Olfactory-pit cilia movement in WT zebrafish and *rsph9* morphants. Top panel: 18.2% (Moex2), 22.2% (MOex3), and 0.8% (MOex2 + *rsph9* mRNA) of cilia in morphants were immotile (1.4% in WT). Middle panel: 65.9% (MOex2), 65.6% (MOex3), and 7% (MOex2 + *rsph9* mRNA) of cilia were dysmotile (3.1% in WT), this number including that which was immotile in addition to dysmotile; i.e., displaying an ineffective circular beat pattern. Bottom panel: cilia beat frequency was unaffected at 42.3 Hz (MOex2), 40.0 Hz (MOex3), and 39.8 Hz (MOex2 + *rsph9* mRNA) (WT 43.6 Hz). Means ± SEM from seven WT, eight MOex2, nine MOex3 and five MOex2 plus coinjected *rsph9* mRNA embryos are shown. Triple asterisk indicates p < 0.001.

(B) Accumulation of debris in *rsph9* zebrafish morphant olfactory pit. Top panel, 72 hpf zebrafish, indicating nasal pit in relation to the eye (arrowhead). Bottom left panel: representative example of 72 hpf *rsph9* MOex3 morphant zebrafish with debris accumulation evident in the nasal pit (arrows). Bottom right panel: WT zebrafish showing normal debris clearance due to fluid vortex created by cilia beating. MOex2 showed the same defect (not shown).

(C) *Chlamydomonas* flagella movement in WT (*cw15*) and in *pf17*, *pf17*-T and *pf17*-Tmut strains. Top: flagella motility was within the normal range at 4.6% in *pf17*-T, but in *pf17*-Tmut, 73.0% of flagella were immotile, compared to 1.0% in WT and 99.8% in *pf17*. Bottom: flagella beat frequency was within the normal range at 53.5 Hz in *pf17*-T, but reduced to 24.9 Hz in *pf17*-Tmut (WT 47.9 Hz, *pf17* 0.0 Hz). Shown are means ± SEM from 5–10 cells (immotility index) or 20–26 cells (flagellar beat frequency [FBF]). Triple asterisk indicates p < 0.001.

beat pattern (66% cilia dysmotile) (Figure 4A and Movies S1–S3). Statistical comparison between data sets indicated that the II and DI for both sets of MO-injected embryos were significantly higher than that observed for controls (p < 0.001). Morphants had a more static fluid flow than did WT, and this allowed debris to accumulate in the pits (Figure 4B and Movies S1–S3). Their beat pattern resembled that of cilia in *RSPH* patients, confirming that ablating gene expression causes similar cilia-dysmotility defects. This effect was rescued by coinjection of mouse *Rsph9* mRNA, which restored the normal beat pattern (Figure 4A).

Comparison at 24 and 48 hpf between morphant zebrafish (n = 163 exon 2, 163 exon 3) and WT zebrafish (n = 270) showed that laterality was unaffected. Three of the exon 3 morphants, none of the exon 2 morphants, and one WT fish displayed *situs inversus*, which was a nonsignificant difference. S*itus inversus* presents occasionally as a well-recognized "background" zebrafish phenotype (L.R and S.W.W., unpublished data).

The *Chlamydomonas* mutant strain *pf17* has a mutation in *RSP9*, the ortholog of human *RSPH9*, resulting in immotile flagella. The entire radial spoke head complex is absent, and there is central-pair displacement, rather than loss.[42] We first determined that *pf17* carries a single-bp deletion, c.131delG, in *RSP9*, predicting an early premature stop codon (p.Ser45AlafsX3). We then used the presumed

Rsp9 null background of the *pf17* strain to investigate the effects of the human *RSPH9* p.Lys268 del mutation. We stably transformed *pf17* with the WT *RSP9* gene to create the strain *pf17*-T. *pf17*-T regained a normal beat velocity and pattern, indicating complete phenotype rescue (Figure 4C and Movies S4–S7). We then stably transformed *pf17* with a mutated version of *RSP9* carrying the equivalent of the 3 bp p.Lys268del deletion to create the strain *pf17*-Tmut. Statistical comparison between data sets indicated that the FBF for *pf17*-Tmut was significantly reduced and the II significantly increased, compared to controls (p < 0.001). Therefore, *pf17*-Tmut showed only partial rescue, with a beat velocity at half the WT level and flagella either immotile (73% immotile) or displaying a slowed, disorganized beat ineffective for normal movement (Figure 4C and Movies S4–S7). Differences in flagella and cilia movement preclude rigorous comparisons of beat pattern. Thus, recreation of the human *RSPH9* mutation in *Chlamydomonas* provides direct evidence of its pathogenic effect on motility of cilia and flagella.

Discussion

We have identified mutations in two genes encoding radial spoke head proteins, *RSPH9* and *RSPH4A*, in PCD families that have defects of the central microtubular pair. This is the first report of PCD genes that cause disease associated with cilia-axoneme defects other than a loss or reduction of the outer dynein arms. Using model organisms, we have also shown that *Rsph9* is expressed in ciliated epithelia and that gene knockdown and mimicking of the human *RSPH9* p.Lys268 del mutation recapitulates its detrimental effect on cilia motility.

Analysis of *Chlamydomonas RSP9* mutant strains indicates that the human *RSPH9* p.Lys268 del mutation is likely to be hypomorphic, given that some flagella function is retained in these mutants, in contrast to those with a null allele. RSPH9 residue Lys268 is conserved in all mammals, but not in some of the nonvertebrates and ciliates tested. This could reflect a functional distinction among the cilia of different species, or it could be that the loss of this amino acid, rather than its specific chemical properties, is what confers the disease-causing effect. Although the p.Lys268 del mutation was detected on 0.7% of control chromosomes, it was never present in a homozygous state in the control individuals, whereas sequencing of the entire open reading frame in affected patients showed that they were all homozygous for this single mutation. The population frequency of the mutant allele is not significantly different from what is expected of a pathogenic recessive mutation. Additionally, the majority of control chromosomes were sampled from the highly consanguineous UAE population, from which one family carrying the mutation (UCL146) originates. These observations support the idea that the p.Lys268 del mutation is disease causing.

We expect that the three premature nonsense mutations that we have identified in *RSPH4A* are more likely to be null alleles, because they are predicted to result in premature protein truncation, but this requires further functional work for confirmation. These *RSPH4A* nonsense mutations predict a disruption of the "radial spoke domain" (Figure S2B). No other functional domains could be identified by computer modeling in either of the two radial spoke head proteins, although RSPH4A orthologs are noted as proline rich,[43] thereby preventing significant genotype-phenotype predictions.

Determination of ultrastructural changes in the axoneme is limited by methodological constraints. In particular, observations reflect a sampling of total tissue such that local changes in ciliary structure might be missed. The observed structural changes appear to vary according to species, organelle type, protein involved, and specific mutation. Truncation mutations in *RSPH4A* in human motile cilia are associated with a loss of the central pair, yet for an *RSP9* truncation mutation in *Chlamydomonas pf17*, the central pair is retained but displaced. The different contribution of RSPH4A and RSPH9 proteins to the spoke-head structure is not clear. Furthermore, it is not yet known whether differences in central-pair structural constraints and waveform between cilia and flagella could explain the disparity or whether the human patients might have more intact and functionally preserved radial spoke heads than the *Chlamydomonas* mutants. In humans with a single-aa deletion in *RSPH9*, the structural consequences are distinct, with only a localized loss of the central-pair microtubules, perhaps reflecting the predicted milder mutation. Of the two families with the *RSPH9* p.Lys268 del mutation, a normal central-pair ultrastructure was in fact recorded in family UCL152, but in view of the shared mutation in common with UCL146, it seems likely that the minor central-pair defect observed in UCL146 could have missed detection in UCL152 without the more detailed sampling that was undertaken in UCL146, which included generation of longitudinal sections.[20]

The functional consequences that we have observed arising from *RSPH9* and *RSPH4A* defects in patients and model organisms support a more significant role for radial spoke heads and central-pair microtubules in determining cilia beat waveform rather than velocity, although velocity may also be affected. This is consistent with the observed retention of the force-generating dynein arms that govern velocity in the cilia axonemes of central-pair-defect patients. The natural movement of 9+2 motile cilia and 9+0 nodal cilia differs: the 9+0 cilium has a circular motion, rather than the planar "whiplash" movement of 9+2 cilia, with effective and recovery strokes.[7,44] In zebrafish and *RSPH9* and *RSPH4A* patients, altered function of the radial spoke heads caused 9+2 cilia motility to resemble this simpler rotary 9+0 cilia movement. This is consistent with previous evidence that a disconnection of radial spoke head central-pair interactions in 9+2 cilia would lead to a change from the normal planar motion

to abnormal movement.[39,41] For example, an antibody to sea urchin RSPH4A was previously shown to affect sperm-flagella beat pattern but not velocity, changing the movement from planar to circular.[45]

The normal laterality observed in *RSPH9* and *RSPH4A* patients and *rsph9* zebrafish morphants is consistent with the notion that radial spoke proteins are not essential for nodal ciliary function. Their role in waveform appears more important in central-pair-containing 9+2 cilia. Our observation from in situ hybridization, that *Rsph9* is expressed in mouse nodal cilia (which lack a central pair), suggests either redundancy or an alternative, perhaps structural, role. The precise function of the radial spoke head proteins at the embryonic node is likely to be relevant to the molecular basis of the difference in 9+0 node cilia and 9+2 motile cilia waveforms and remains of considerable interest. However, many unresolved questions remain concerning the correlation of structure and function in different cilia types.

In summary, our observations provide new insights into the role of radial spoke head proteins in the structure and function of cilia and flagella and in the molecular genetic basis of primary ciliary dyskinesia. *RSPH9* and *RSPH4A* represent good candidate disease-causing genes for cases of PCD with central-pair defects and also for cases in which the axonemal dynein arms are retained and the patients do not display laterality defects. Characterization of *RSPH9* and *RSPH4A* and continuing elucidation of the molecular basis of PCD provide new opportunities for noninvasive diagnosis and the possibility of new therapies in what we have shown is, at least in some model organisms, a reversible (rescuable) molecular defect.

Supplemental Data

Supplemental Data include four figures, one table, and seven movies and can be found with this article online at http://www.ajhg.org/.

Web Resources

The URLs for data presented herein are as follows:

Chlamydomonas Center, http://www.chlamy.org/
Ensembl, http://www.ensembl.org/
European Collection of Cell Cultures, http://www.ecacc.org.uk/
National Laboratory for the Genetics of Israeli Populations, http://nlgip.tau.ac.il/
NCBI, http://www.ncbi.nlm.nih.gov
Online Mendelian Inheritance in Man (OMIM), http://ncbi.nlm.nih.gov/Omim/
UCSC Genome Browser, http://genome.ucsc.edu

References

1. Bush, A., Chodhari, R., Collins, N., Copeland, F., Hall, P., Harcourt, J., Hariri, M., Hogg, C., Lucas, J., Mitchison, H.M., et al. (2007). Primary ciliary dyskinesia, current state of the art. Arch. Dis. Child. *92*, 1136–1140.
2. Rott, H.D. (1979). Kartagener's syndrome and the syndrome of immotile cilia. Hum. Genet. *46*, 249–261.
3. Jeganathan, D., Chodhari, R., Meeks, M., Faeroe, O., Smyth, D., Nielsen, K., Amirav, I., Luder, A.S., Bisgaard, H., Gardiner, R.M., et al. (2004). Loci for primary ciliary dyskinesia map to chromosome 16p12.1–12.2 and 15q13.1–15.1 in Faroe Islands and Israeli Druze genetic isolates. J. Med. Genet. *41*, 233–240.
4. O'Callaghan, C. (2004). Innate pulmonary immunity, cilia. Pediatr. Pulmonol. *26* (*Suppl*.), 72–73.
5. Kosaki, K., Ikeda, K., Miyakoshi, K., Ueno, M., Kosaki, R., Takahashi, D., Tanaka, M., Torikata, C., Yoshimura, Y., and Takahashi, T. (2004). Absent inner dynein arms in a fetus with familial hydrocephalus-situs abnormality. Am. J. Med. Genet. A. *129A*, 308–311.
6. Ibanez-Tallon, I., Pagenstecher, A., Fliegauf, M., Olbrich, H., Kispert, A., Ketelsen, U.P., North, A., Heintz, N., and Omran, H. (2004). Dysfunction of axonemal dynein heavy chain Mdnah5 inhibits ependymal flow and reveals a novel mechanism for hydrocephalus formation. Hum. Mol. Genet. *13*, 2133–2141.
7. Nonaka, S., Tanaka, Y., Okada, Y., Takeda, S., Harada, A., Kanai, Y., Kido, M., and Hirokawa, N. (1998). Randomization of left-right asymmetry due to loss of nodal cilia generating leftward flow of extraembryonic fluid in mice lacking KIF3B motor protein. Cell *95*, 829–837.
8. Kennedy, M.P., Omran, H., Leigh, M.W., Dell, S., Morgan, L., Molina, P.L., Robinson, B.V., Minnix, S.L., Olbrich, H., Severin, T., et al. (2007). Congenital heart disease and other heterotaxic defects in a large cohort of patients with primary ciliary dyskinesia. Circulation *115*, 2814–2821.
9. Loges, N.T., Olbrich, H., Fenske, L., Mussaffi, H., Horvath, J., Fliegauf, M., Kuhl, H., Baktai, G., Peterffy, E., Chodhari, R., et al. (2008). *DNAI2* mutations cause primary ciliary dyskinesia with outer dynein arm defects. Am. J. Hum. Genet., in press. Am. J. Hum. Genet. *83*, 547–558.

10. Bush, A., Hogg, C., Mitchison, H.M., Nisbet, M., and Wilson, R. (2008). Update in primary ciliary dyskinesia. Clin. Pulm. Med., in press.

11. Hornef, N., Olbrich, H., Horvath, J., Zariwala, M.A., Fliegauf, M., Loges, N.T., Wildhaber, J., Noone, P.G., Kennedy, M., Antonarakis, S.E., et al. (2006). DNAH5 mutations are a common cause of primary ciliary dyskinesia with outer dynein arm defects. Am. J. Respir. Crit. Care Med. *174*, 120–126.

12. Zariwala, M.A., Leigh, M.W., Ceppa, F., Kennedy, M.P., Noone, P.G., Carson, J.L., Hazucha, M.J., Lori, A., Horvath, J., Olbrich, H., et al. (2006). Mutations of DNAI1 in primary ciliary dyskinesia, evidence of founder effect in a common mutation. Am. J. Respir. Crit. Care Med. *174*, 858–866.

13. Failly, M., Saitta, A., Munoz, A., Falconnet, E., Rossier, C., Santamaria, F., de Santi, M.M., Lazor, R., Delozier-Blanchet, C.D., Bartoloni, L., and Blouin, J.L. (2008). *DNAI1* Mutations Explain Only 2% of Primary Ciliary Dykinesia. Respiration *76*, 198–204.

14. Meeks, M., Walne, A., Spiden, S., Simpson, H., Mussaffi-Georgy, H., Hamam, H.D., Fehaid, E.L., Cheehab, M., Al-Dabbagh, M., Polak-Charcon, S., et al. (2000). A locus for primary ciliary dyskinesia maps to chromosome 19q. J. Med. Genet. *37*, 241–244.

15. Geremek, M., Schoenmaker, F., Zietkiewicz, E., Pogorzelski, A., Diehl, S., Wijmenga, C., and Witt, M. (2008). Sequence analysis of 21 genes located in the Kartagener syndrome linkage region on chromosome 15q. Eur. J. Hum. Genet. *16*, 688–695.

16. Geremek, M., and Witt, M. (2004). Primary ciliary dyskinesia, genes., candidate genes and chromosomal regions. J. Appl. Genet. *45*, 347–361.

17. Moore, A., Escudier, E., Roger, G., Tamalet, A., Pelosse, B., Marlin, S., Clement, A., Geremek, M., Delaisi, B., Bridoux, A.M., et al. (2006). RPGR is mutated in patients with a complex X linked phenotype combining primary ciliary dyskinesia and retinitis pigmentosa. J. Med. Genet. *43*, 326–333.

18. Saeki, H., Kondo, S., Morita, T., Sasagawa, I., Ishizuka, G., and Koizumi, Y. (1984). Immotile cilia syndrome associated with polycystic kidney. J. Urol. *132*, 1165–1166.

19. Budny, B., Chen, W., Omran, H., Fliegauf, M., Tzschach, A., Wisniewska, M., Jensen, L.R., Raynaud, M., Shoichet, S.A., Badura, M., et al. (2006). A novel X-linked recessive mental retardation syndrome comprising macrocephaly and ciliary dysfunction is allelic to oral-facial-digital type I syndrome. Hum. Genet. *120*, 171–178.

20. Stannard, W., Rutman, A., Wallis, C., and O'Callaghan, C. (2004). Central microtubular agenesis causing primary ciliary dyskinesia. Am. J. Respir. Crit. Care Med. *169*, 634–637.

21. Cadenas, A.M., Zhivotovsky, L.A., Cavalli-Sforza, L.L., Underhill, P.A., and Herrera, R.J. (2008). Y-chromosome diversity characterizes the Gulf of Oman. Eur. J. Hum. Genet. *16*, 374–386.

22. Abecasis, G.R., Cherny, S.S., Cookson, W.O., and Cardon, L.R. (2002). Merlin–rapid analysis of dense genetic maps using sparse gene flow trees. Nat. Genet. *30*, 97–101.

23. Hoffmann, K., and Lindner, T.H. (2005). easyLINKAGE-Plus–automated linkage analyses using large-scale SNP data. Bioinformatics *21*, 3565–3567.

24. Kruglyak, L., and Lander, E.S. (1998). Faster multipoint linkage analysis using Fourier transforms. J. Comput. Biol. *5*, 1–7.

25. Altschul, S.F., Madden, T.L., Schaffer, A.A., Zhang, J., Zhang, Z., Miller, W., and Lipman, D.J. (1997). Gapped BLAST and PSI-BLAST, a new generation of protein database search programs. Nucleic Acids Res. *25*, 3389–3402.

26. Pazour, G.J., Agrin, N., Leszyk, J., and Witman, G.B. (2005). Proteomic analysis of a eukaryotic cilium. J. Cell Biol. *170*, 103–113.

27. Stolc, V., Samanta, M.P., Tongprasit, W., and Marshall, W.F. (2005). Genome-wide transcriptional analysis of flagellar regeneration in Chlamydomonas reinhardtii identifies orthologs of ciliary disease genes. Proc. Natl. Acad. Sci. USA *102*, 3703–3707.

28. Broadhead, R., Dawe, H.R., Farr, H., Griffiths, S., Hart, S.R., Portman, N., Shaw, M.K., Ginger, M.L., Gaskell, S.J., McKean, P.G., et al. (2006). Flagellar motility is required for the viability of the bloodstream trypanosome. Nature *440*, 224–227.

29. El-Sayed, N.M., Myler, P.J., Blandin, G., Berriman, M., Crabtree, J., Aggarwal, G., Caler, E., Renauld, H., Worthey, E.A., Hertz-Fowler, C., et al. (2005). Comparative genomics of trypanosomatid parasitic protozoa. Science *309*, 404–409.

30. Olbrich, H., Haffner, K., Kispert, A., Volkel, A., Volz, A., Sasmaz, G., Reinhardt, R., Hennig, S., Lehrach, H., Konietzko, N., et al. (2002). Mutations in DNAH5 cause primary ciliary dyskinesia and randomization of left-right asymmetry. Nat. Genet. *30*, 143–144.

31. Ybot-Gonzalez, P., Copp, A.J., and Greene, N.D. (2005). Expression pattern of glypican-4 suggests multiple roles during mouse development. Dev. Dyn. *233*, 1013–1017.

32. Lai, C.S., Gerrelli, D., Monaco, A.P., Fisher, S.E., and Copp, A.J. (2003). FOXP2 expression during brain development coincides with adult sites of pathology in a severe speech and language disorder. Brain *126*, 2455–2462.

33. Chilvers, M.A., and O'Callaghan, C. (2000). Analysis of ciliary beat pattern and beat frequency using digital high speed imaging, comparison with the photomultiplier and photodiode methods. Thorax *55*, 314–317.

34. Harris, E. (1989). The *Chlamydomonas* Sourcebook. A Comprehensive Guide to Biology and Laboratory Use (San Diego: Academic Press).

35. Goldschmidt-Clermont, M., Girard-Bascou, J., Choquet, Y., and Rochaix, J.D. (1990). Trans-splicing mutants of Chlamydomonas reinhardtii. Mol. Gen. Genet. *223*, 417–425.

36. Davies, J.P., and Grossman, A.R. (1994). Sequences controlling transcription of the Chlamydomonas reinhardtii beta 2-tubulin gene after deflagellation and during the cell cycle. Mol. Cell. Biol. *14*, 5165–5174.

37. Kindle, K.L. (1990). High-frequency nuclear transformation of Chlamydomonas reinhardtii. Proc. Natl. Acad. Sci. USA *87*, 1228–1232.

38. Abdulrazzaq, Y.M., Bener, A., al-Gazali, L.I., al-Khayat, A.I., Micallef, R., and Gaber, T. (1997). A study of possible deleterious effects of consanguinity. Clin. Genet. *51*, 167–173.

39. Yang, P., Diener, D.R., Yang, C., Kohno, T., Pazour, G.J., Dienes, J.M., Agrin, N.S., King, S.M., Sale, W.S., Kamiya, R., et al. (2006). Radial spoke proteins of Chlamydomonas flagella. J. Cell Sci. *119*, 1165–1174.

40. Porter, M.E., and Sale, W.S. (2000). The 9 + 2 axoneme anchors multiple inner arm dyneins and a network of kinases and phosphatases that control motility. J. Cell Biol. *151*, F37–F42.

41. Smith, E.F., and Yang, P. (2004). The radial spokes and central apparatus, mechano-chemical transducers that regulate flagellar motility. Cell Motil. Cytoskeleton *57*, 8–17.

42. Huang, B., Piperno, G., Ramanis, Z., and Luck, D.J. (1981). Radial spokes of Chlamydomonas flagella, genetic analysis of assembly and function. J. Cell Biol. *88*, 80–88.

43. Curry, A.M., Williams, B.D., and Rosenbaum, J.L. (1992). Sequence analysis reveals homology between two proteins of the flagellar radial spoke. Mol. Cell. Biol. *12*, 3967–3977.

44. Chilvers, M.A., Rutman, A., and O'Callaghan, C. (2003). Ciliary beat pattern is associated with specific ultrastructural defects in primary ciliary dyskinesia. J. Allergy Clin. Immunol. *112*, 518–524.

45. Gingras, D., White, D., Garin, J., Cosson, J., Huitorel, P., Zingg, H., Cibert, C., and Gagnon, C. (1998). Molecular cloning and characterization of a radial spoke head protein of sea urchin sperm axonemes, involvement of the protein in the regulation of sperm motility. Mol. Biol. Cell *9*, 513–522.